Simulating random alloy effects in III-nitride light emitting diodes

A. Di Vito,[1] A. Pecchia,[2] A. Di Carlo,[1, a)] and M. Auf der Maur[1, b)]
[1)]*Dept. Electronic Engineering, University of Rome Tor Vergata, Via Politecnico 1, 00133 Rome, Italy*
[2)]*CNR-ISMN, Via Salaria Km. 29.300, 00017 Monterotondo, Rome, Italy*

(Dated: 7 July 2020)

Statistical fluctuations in the alloy composition on the atomic scale can have important effects on electronic and optical properties of bulk materials and devices. In particular, carrier localization induced by alloy disorder has been a much discussed topic during the last decade with regard to III-nitride light emitting diodes (LEDs). Many experimental and theoretical work has been dedicated to the study of the effects of alloy disorder on carrier localization and finally on the efficiency and transport properties in such devices. Modeling approaches range from empirical analytical models down to atomistic ab-initio ones, each with its advantages and disadvantages. In this tutorial we discuss the simulation of alloy fluctuations in nitride quantum well LEDs by combining continuum device models and an atomistic empirical tight binding model, which provides a suitable compromise between atomic precision and computational effort.

I. INTRODUCTION

The downscaling of device dimensions has led to a paradigm shift in the way we simulate devices. As a matter of fact, quantum mechanical effects, such as confinement, coherency or tunneling, become more and more important when the feature size of devices is of few tens of nanometers or less. On the other hand, the most used and effective model for electronic transport is based on the drift-diffusion approximation, that means on the assumptions of diffusive, scattering dominated transport and local thermal equilibrium. Thus, in order to address quantum mechanical and/or non-equilibrium effects, a wide range of approaches has been developed in the last decades, like quantum corrected drift-diffusion and hydrodynamic models, Schrödinger/drift-diffusion[1], quantum corrected Monte Carlo[2], Wigner Monte Carlo[3] and non-equilibrium Green's function (NEGF) approaches[4].

The miniaturization process is regarding transistor devices as well as optoelectronic ones and the characteristic device dimension has reached the nanometer scale. As a consequence, additional effects come into play due to the underlying atomistic structure. In fact, crystal defects, impurities, position of dopants, random fluctuations of alloy composition and other details of the atomic disposition become relevant at such small length scales and need to be taken into account in the device simulation. Atomistic models are therefore required[5] in order to consider such features, that cannot be resolved by continuous media models, like elasticity and drift-diffusion, or by quantum mechanical models based on the envelope function approximation, such as typical k·p based implementations. Moreover, atomistic approaches allow to consider the interaction of atoms at the interface between different materials. This is paramount in structures where interface properties are expected to affect the device behaviour. As an example, in nitride based quantum wells (QWs) the polarization induced built-in electric field leads to severe quantum-confined Stark effect (QCSE)[6]. In this case, the electron and hole states are localized close to the QW interfaces and experience non-idealities of the interface microstructure, that usually deviates from the ideal flat QW.

However, atomistic models are computationally expensive and only the active region of the device can usually be treated atomistically. Thus, a consistent connection between the atomistic and the continuous media models is required in order to be able to simulate a whole electronic device. As an example, the properties of the active region are expected to be influenced by the interaction with other parts of the device by means of strain or electromagnetic interaction. Multiscale approaches are therefore the new simulation paradigm that allows to combine the advantages of both continuous and atomistic methods in a consistent multiscale setup[7–13].

In the following, we focus on the multiscale simulation of light emitting diodes (LEDs) based on indium gallium nitride (InGaN). In fact, InGaN is a successful material for the realization of efficient short-wavelength commercial LEDs[14–16]. Although the technology for InGaN based blue and white LEDs has been successfully commercialized, there are several material related issues, such as efficiency droop, green gap, compositional non-uniformity and spatial localization of carriers, which are still under debate[17–30].

While structural characterisation reveals a compositional uniformity compatible with the assumption of a random alloy in high quality structures[31], one should expect some deviation from such an idealized structure on the atomic scale. Previous studies show that the fluctuations in the local indium concentration, even in the case of a uniform random alloy, lead to translational symmetry breaking and carrier spatial localization[29,32–36]. Interestingly, the hole localization, particularly evident in samples containing indium clusters, appears to have a strong influence on the alloy properties[37,38]. In most of the studies conducted so far, the impact of deviations from a uniform random alloy on the properties of InGaN has not been discussed[19,20,27,32,33,39]. Furthermore, the theoretical analysis based on density functional theory (DFT) performed on clustered InGaN bulk structures[40,41] lack a properly large supercell size and a sufficiently large number of random samples. In fact, the periodically repeated supercell introduces an artificial periodicity, which may interfere with a correct interpretation of the results if the supercell size is in the order of or

[a)]Also at CNR-ISM, Via del Fosso del Cavaliere 100, 00133 Rome, Italy
[b)]Electronic mail: auf.der.maur@ing.uniroma2.it

smaller than the characteristic localization length.

The role of clustering for the properties of InGaN alloys and the performances of InGaN based LEDs, supported by a proper statistical characterization of the samples, has recently been discussed[24,25]. Based on these results, we demonstrate how the combination of atomistic and continuous models allows to describe the effects of compositional non-uniformity on the performance of InGaN based LEDs.

In Section II, we give a brief description of continuous and atomistic methods used to model alloy disorder. In Section III, we discuss some aspects of multiscale approaches for the coupling of atomistic and continuous models, focusing on their application to III-nitride LED modeling. Then, in Section IV, we show several examples of InGaN based LED simulations, where using such schemes can help in getting more insight into device behaviour and in interpreting experimental findings.

II. MODELING ALLOY DISORDER IN NITRIDES

A. Continuum models

The most used approach to simulate electronic states and optical properties in quantum well devices is using a continuum description of the relevant regions, based on k·p theory[42–44]. The electronic states in this case are expanded in bulk Bloch states, which are assumed to be modulated by envelope functions that vary slowly with respect to the electron or hole wavelengths. Putting this expansion into the Schrödinger equation, and keeping explicitly only the bands of interest, leads to a set of equations for the envelope functions. For III-nitrides, usually an 8-band approximation is used, which includes the lowest conduction band and three valence bands.

The solution of the eigenstates of the k·p Hamiltonian can be done very efficiently, especially in one dimensional systems like planar heterostructures, so that self-consistent Schrödinger/Poisson/drift-diffusion simulations are easily performed. Even 2D and 3D simulations are feasible.

Since k·p has no awareness of the underlying atomic structure, there is no unique recipe on how to include disorder on the atomic scale for the description of alloys. Instead, disorder has to be included a posteriori, e.g. by adding band tails to the density of states, or by introducing spatially varying alloy concentrations. The definition of the latter, however, at first is largely arbitrary, because the local mean alloy concentration is obtained by counting atoms in a certain control volume. This volume is not well defined and should depend on the spatial volume on which the carriers' probability density is different from zero. Therefore, an additional parameter enters into the model, and it must be expected that the simulation results depend to some extent on the choice of this parameter. This is illustrated in Fig. 1, which shows the local mean indium concentration at the center of a 4 nm thick $In_{0.25}Ga_{0.75}N$/GaN QW with roughly 10×10 nm^2 in-plane supercell, using different radii for the spherical control volumes from roughly 0.33 nm to 1 nm, containing a total of 14 to 187 cations. This number is fixed for each control volume position, in order to get a consistent statistical distribution.

It can be observed that the statistical width of the distribution of the local indium concentration strongly depends on the control volume radius. The effect on the calculated electronic states is shown in Fig. 2. In the figure we show the electron and hole ground state wave functions and the ground state energies in the same InGaN QW under flat band conditions, calculated with k·p for different control volume radii. It can be observed that both ground state energies vary with decreasing control volume radius, leading to a decrease in band gap. This is accompanied by a change in localisation, which results also in a modification of the wave function overlap. A suitable radius for the control volume for the calculation of the local alloy composition should ideally be determined by comparing with atomistic models. Note, however, that this radius might be different for electrons and holes, and for different states.

Nevertheless, k·p based simulations on spatially non-uniform indium concentrations have been successfully performed during the past, leading to important insight into the effects of alloy fluctuations in III-nitride QWs[30].

Similarly, empirical models have been employed to explain for example the measured thermal behaviour of the recombination coefficients in green InGaN/GaN LEDs[26,37,45].

In more recent years, an additional, novel approach to treat disordered systems has been proposed, which is based on the so called potential landscape theory[28,46,47]. In this model, the diagonalization of the Hamiltonian can be circumvented by introducing an effective potential, obtained from a linear boundary value problem, that leads to a very good approximation of the density of states. This approach is currently used for the 3D simulation of transport in multi-QW LEDs[48,49].

In order to deduce electronic and optical properties directly from the atomic structure, without the introduction of further empirical parameters, it is desirable though to resort to models that take the atomic structure into account.

B. Ab-initio methods

Ab-initio or first-principles methods based on density functional theory (DFT) do not require adjustable input parameters to perform the simulations. They offer an accurate atomistic representation of the system under investigation. However, accurate models based on hybrid functionals[50], GW[51] and BSE[52] approximations are computationally too expensive to be applied in device simulations, where the active region is typically composed of millions of atoms. On the other hand, less expensive ab-initio methods based on the local density approximations (LDA) or generalized gradient approximations (GGA)[53] do not reproduce experimental band gaps, relative band offsets and effective masses accurately enough.

Since simulations including non-uniformities in the atomic configuration, like random alloy or quantum well thickness fluctuations, require relatively large supercells with ten thousands and more atoms, density functional based approaches become inapplicable, and empirical models on the basis of localized atomic orbitals become a suitable alternative.

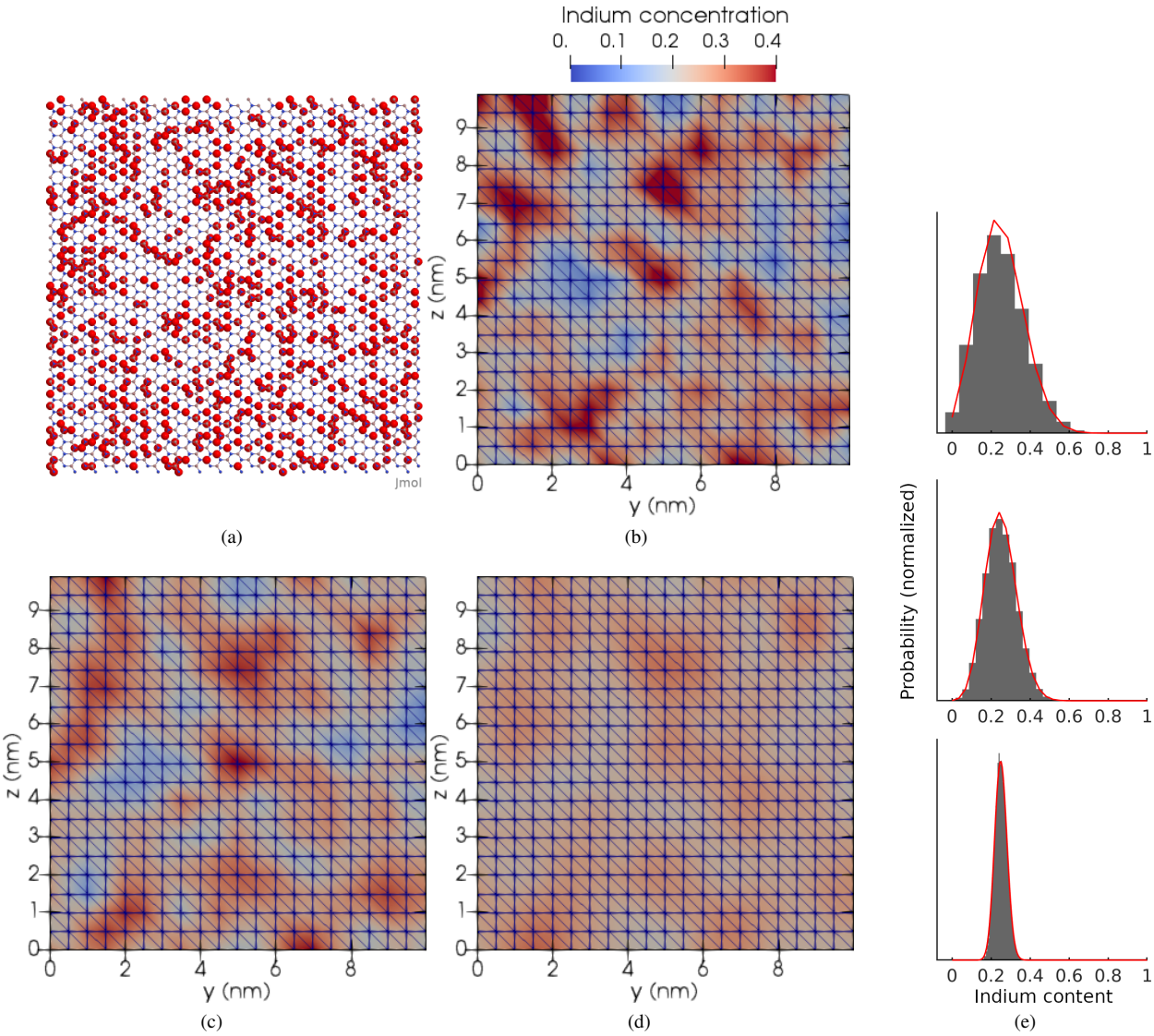

FIG. 1. a) The atomic structure of the InGaN QW, including only the central three monolayers. Indium atoms are evidenced in red. b) Indium concentration on the central plane of the QW, for 0.33 nm control volume radius. The same for 0.5 nm (c) and 1 nm (d) radius. The finite element mesh is indicated in panels b)-d), and the color scale is the same for all. In e) the distributions of the local indium concentration is reported for the three control volume radii (0.33 nm at top to 1 nm at bottom). The red line is the theoretical distribution for a random alloy.

C. Tight binding

ETB[54,55] represents a good trade-off between accuracy and computational burden. It is widely used for device applications, since it allows to simulate structures composed of millions of atoms, combining numerical efficiency with reasonably accurate results[56]. In the TB approach, the wave function is expressed as a linear combination of localized atomic orbitals. This is a natural choice, since we want to describe systems with atomic resolution, where transport bands are formed by the interaction of atomic orbitals. Moreover, using localized atomic orbitals is a suitable choice to analyze confined systems and to study properties based on localized features, such as impurities or alloy disorder[57].

However, a good representation of a physical system by means of a TB approach requires an accurate parameterization of the Hamiltonian matrix elements. This is usually done by fitting over suitable properties of the system that can be measured by experiments or computed with more accurate approaches. Band dispersions of bulk reference materials are one of the typical targets in these fittings, useful for electronic simulations. For this reason we refer to the method as 'empirical' TB.

The choice of TB basis can be the minimal sp^3 set, sufficient to approximate the valence bands. Spin-orbit coupling is included as an intra-atomic potential coupling spin with angular momentum, as shown by Chadi[58], which doubles the Hamiltonian size. However, in order to reproduce the full

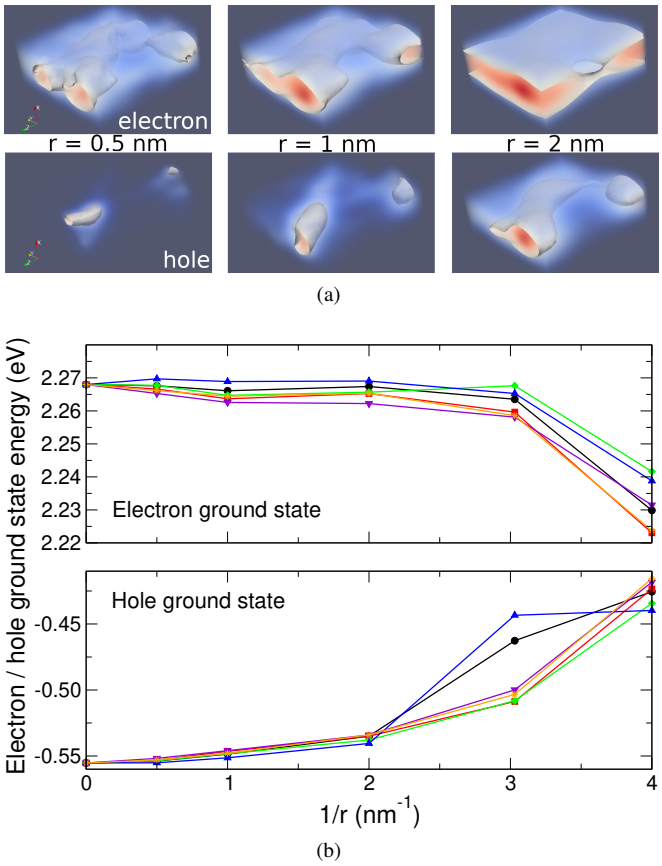

FIG. 2. The electron and hole ground state wave functions (a) and energies (b), calculated in 3D with k·p for a random alloy single 4 nm thick $In_{0.25}Ga_{0.75}N$ QW and for different control volume radii r to extract the local indium concentration. Flat band conditions have been used (neglecting polarisation fields) in order to include only the effect of the spatial smoothing on k·p parameters (direct and indirect via strain). The different colors/symbols in (b) are for 5 different random configurations. The black configuration corresponds to the one in Fig. 1.

band of semiconductors or indirect gaps, it is necessary to include 2nd or 3rd neighbor interactions or three center terms, typically not included in the simple Slater-Koster two center representation of the Hamiltonian. In order to retain the two-center approximation and the nearest-neighbor interactions while keeping an accurate representation of the bands, the basis can be extended to sp^3s^* or $sp^3s^*d^5$, increasing the matrix size.

The decomposition into irreducible representations of the T_d point group at Γ-point and along the reciprocal directions <111> $\rightarrow 2\Gamma_1 + 2\Gamma_4$ and along <200> $\rightarrow \Gamma_1 + \Gamma_3 + \Gamma_4$ suggests that the inclusion of a full set of five atomic d-states (Γ_3 and Γ_4 symmetries) is the better choice for the numerical completion of the Hamiltonian. This leads to the 40-bands TB model characteristic of the spds* basis[59,60].

The atomic orbitals are treated as an orthonormal basis set, which is typically justified on the theoretical ground of Wannier orbitals. The orthogonal basis makes the calculations of the eigenstates much easier, but such an approximation must be taken with care, especially with large strains. In fact, structural and bond deformations are treated by fitting the exponents of Harrison-like scaling laws of the two-center matrix elements as, $V_{ijk}=V^0_{ijk}(\frac{d_0}{d})^{\eta_{ijk}}$. However this treatment might give inaccurate results for large deviations of the bond lengths, d, from the reference value, d_0. Efforts to include non-orthogonal corrections, at least as a renormalization of the diagonal elements, have been made in the past[61], but introduce many more parameters in the model. Altogether, in order to parameterize a material such as GaN, we need 4 on-site energies per atom, 21 symmetry adapted matrix elements (such as $V_{ss\sigma}$, $V_{pp\sigma}$, $V_{pp\pi}$, etc) and 21 scaling parameters. Spin orbit splitting, Δ_{so}, and crystal field splitting, Δ_{cf}, parameters complete the set.

While ETB is still computationally heavier than continuum models like k·p, when applied to nanometer sized structures, it has the important advantage that it does not require an additional parameter to characterize the non-uniformity under study, because the latter is encoded in the atomistic structure itself. Therefore, the effects of the non-uniform atomic ordering will directly lead to results like band edge tails, scattering of optical matrix elements and transition energies. If the underlying model and parameterization is good enough, this would allow for example to deduce details of the nature of the atomic disorder by comparing with measured data.

Comparing with measurement, however, requires that the atomistic simulations are performed under as realistic as possible operating conditions, in terms of strain, temperature or electrostatic potential profile. Therefore the need to combine the atomistic description of the active region of interest of a device with the simulation of the overall device.

The problem of a good parameterization boils down to a good transferability. For instance, when fitting independently InN, GaN or AlN, it might turn out that parameters are inconsistent when treating hetero-interfaces or alloys. For instance, based on the requirement of physical consistency, we expect that the onsite energies of the N atom is the same across III-Nitrides, with little variations. One of such consistent parameterization was obtained by Jancu et al.[59,62].

Electrostatic effects can be treated self-consistently, for instance by approximating point-like atomic charges as derived from electronic states and solving for the potential. In these approaches, it has been shown that ETB is able to even describe screening effects and band-discontinuities at hetero-interfaces[63]. In the same work it was also shown that band offsets approximately apply also to small core-shell spherical structures.

In our non self-consistent treatment, the band discontinuity is imposed as an external potential offset at interfaces. This parameter also plays a crucial role in the treatment of random alloys. In traditional TB, the alloy parameters of, for instance, $In_xGa_{1-x}N$ are built from pure InN and GaN components. A possibility is to average all parameters beforehand, but this procedure does not correctly reproduce bandgap bowings and localization effects. The approach is to assume that bulk parameters can be applied to local environments of each atom. Since cations (Ga, In) are always surrounded by 4 N atoms, the on-site energies and two-centre matrix elements (Ga-N or

In-N) are taken from the corresponding bulk materials. For the anion on-site terms we take a weighted local average between GaN and InN bulk parameters, including the band offset of +0.75 eV of InN with respect to GaN. In practice, if N is surrounded by 4 In ions we apply pure InN parameters and in all other cases we take averages between InN and GaN. Concerning the band offset, we originally used a lower value of +0.5 eV[64,65], but we found that the hole and electron localization are better reproduced for a slightly larger value of +0.75 eV, as discussed below and shown in 5. It should be kept in mind that TB parameters are fitted against bulk properties, hence transferability to small portions of materials or even to few atoms can be considered a model approximation that requires careful validation.

Other approaches have been devised in order to treat alloy disorder in InGaN quantum wells. Schulz *et al.* have developed a model based on the continuum k·p Hamiltonian on top of which the piezoelectric potential is superimposed[66]. This has been later refined using an sp^3 TB model[67–69].

III. COMBINING ATOMISTIC MATERIAL MODELS WITH DEVICE SIMULATION

Since we are mostly interested in simulation results that can be compared with experimental data, it is necessary to perform the simulations under relevant operating conditions. That is, the atomistic model should be embedded into a model of the macroscopic device in a multiscale setup[7,70–72].

The different ways of possible couplings between atomistic and continuous models relevant for LED simulations are schematically shown in Figure 3. Continuous linear elasticity is employed to derive a macroscopic description of mechanical strain. This is very important in III-nitride based structures, due to the pronounced lattice mismatch between the constituents, i.e. (In,Al,Ga)N. In particular, the local strain tensor calculated by linear elasticity is needed to properly define the bulk band edges for the calculation of the carrier densities[43], which in turn influences the electrostatic potential ϕ via the Poisson/drift-diffusion equations. The electrostatic potential finally enters the ETB model via the Hartree term in the device Hamiltonian.

The atomistic structure for ETB is derived from a valence force field (VFF) based relaxation[73], preconditioned by the continuous deformation, as obtained by linear elasticity. In fact, to obtain correct results from ETB, it is paramount to have a proper description of the atomic structure, since strain enters the ETB parameterization by means of a scaling of the off-diagonal Hamiltonian matrix elements, depending on the bond lengths[59], as described in sec. II C. In particular, in an InGaN/GaN system, the relaxed atomic positions strongly deviate from the bulk configuration, as the lattice mismatch between InN and GaN amounts to roughly 10%.

In principle, a self-consistent Schrödinger/Poisson coupling scheme could be employed[63]. However, this becomes unpractical when using ETB on large atomic structures, because of large computation time and the necessity to compute a large number of states. A strategy could be to use a continuum method like k·p to obtain the charge density, in order to approximate the electrostatic potential. However, this approach requires a careful choice regarding the parameterization of the random alloy for the continuum model.

As an alternative to solving the one-particle eigenstates from a k·p or ETB Hamiltonian, an elegant way to treat the quantum mechanical part of the modeling is by means of non-equilibrium Green's functions (NEGF)[74], indicated in Fig. 3 by the red box. This approach allows for an easy implementation of open boundary conditions, and may be more efficient for the calculation of the quantum density in large structures. It can also be used to describe transport in the active region of a LED, including scattering, although the consistent inclusion of non-radiative recombination is rather difficult. Nevertheless, NEGF has been applied to nitride LEDs recently, both based on k·p and ETB[7,75,76].

As mentioned in Section I, the coupling of atomistic and continuous media descriptions is particularly suitable for the simulation of InGaN/GaN LEDs, since it allows to address the presence of compositional non-uniformities in a consistent way. The simulation flow used for the examples presented in the following sections is shown in Fig. 4.

Based on the macroscopic device description, the atomistic structure is generated, using a random, ordered or non-uniform distribution for the alloys, depending on the research topic. Then, continuum strain is solved by linear elasticity, and the mesh and the initial atomistic structure are deformed accordingly. VFF is used to obtain reliable atomic positions. The Poisson/drift-diffusion equations are solved for the operating conditions of interest, e.g. at a typical operating current density in case of a LED. The solution of the electrostatic potential can be improved by using a self-consistent k·p based Schrödinger/drift-diffusion approach in this step. This requires, however, a consistent parameterization of both k·p and ETB. At the end, the electrostatic potential is projected onto the atomic positions, and the required electronic states are calculated from the ETB Hamiltonian. Note that the continuum models can be solved in 1, 2 or 3 dimensions. The LED simulation examples that will be shown are using mostly a 1D approximation, which clearly is computationally more effective, neglecting however potential fluctuations in the QW plane. In principle, using a 3D continuum model[77] is more exact. However, it introduces an uncertainty due to choice on how to project the alloy fluctuations into the continuum, as mentioned in section II A, unless strain, polarization field and carrier densities are all calculated from the atomistic models (see dashed lines from VFF and ETB to the drift-diffusion block in Fig. 4). For the single QW example presented here, the scattering of the ground state eigenvalues for different control volume radii in the projection results to be rather small, as shown in Fig. 5 of the supporting information. We think that the error introduced by the 1D approximation is generally not too severe and does not change qualitatively the main conclusions, at least for not too large degree of clustering and at low carrier densities. Since we are interested in relatively small deviations from the random alloy case, we think this does not invalidate the qualitative results. Nevertheless, one must be aware of the possible spurious effects introduced indirectly

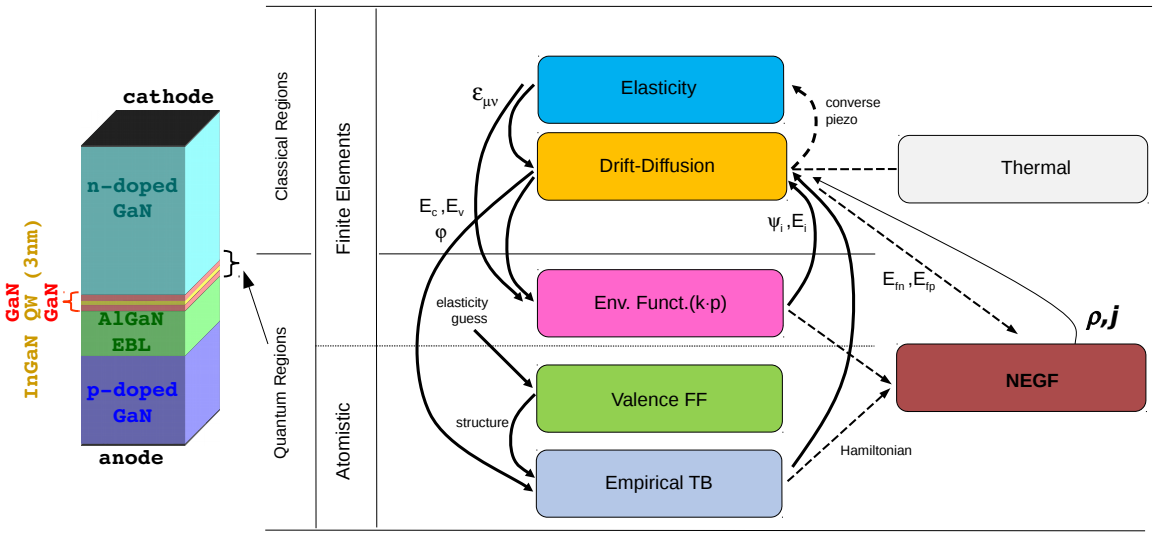

FIG. 3. Quantum/classical and atomistic/continuous coupling schemes for LED simulations. The physical models relevant for LED simulations are represented by rectangular blocks. The quantities used, as parameters or boundary conditions, to connect the models are indicated by arrows. A schematic representation of a simulated LED, with the region treated at the quantum level, is also shown.

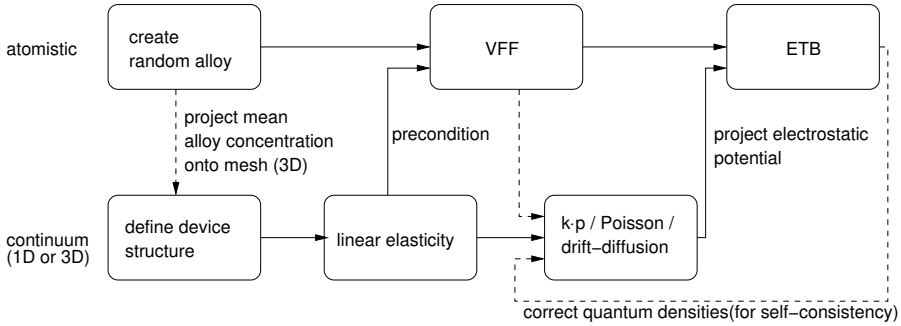

FIG. 4. Simulation flow used for the LED simulations. The self-consistent coupling between ETB and the electrostatic potential has not been performed for the examples.

into the results when using approximate schemes.

IV. SIMULATION EXAMPLES

Experimental and theoretical studies[19,20,32,39,78] have shown that statistical fluctuations in InGaN alloys induce spatial localization of carriers. In particular, the ground state hole wave function is localized within indium rich regions. This effect has a strong influence on the performance of InGaN based LEDs and is further exacerbated by the presence of spatial non-uniformities in the indium content on the nanometer scale. In fact, the presence of indium clusters has been proposed to lead to potential fluctuations that limit the non-radiative recombination of carriers[79]. In recent studies[24,25], a theoretical analysis of the impact of compositional non-uniformity on the electronic and optical properties of the alloy and the device has been performed. In particular, it has been shown that indium clustering induces tail states in both the conduction and valence bands. This causes a reduction of the band gap and a broadening of the optical absorption edge, similar to experimental observation[80]. Furthermore, compositional fluctuations in the active region of the device determine a substantial broadening of the optical emission spectrum and a decrease of the peak emission energy, leading to better agreement with measured spectra. Moreover, the temperature dependence of the radiative coefficient derived for the non-uniform structures is in good agreement with the experimental results[37], that show a temperature behavior opposite to the trend expected from standard theoretical considerations.

Based on these results, we describe here the optical properties of bulk InGaN alloys and InGaN/GaN single-QW (SQW) LEDs, taking into account the statistical fluctuation of the alloy composition and the presence of indium clusters. In particular, we study the transition from a perfect random alloy towards a non-uniform one. The results of the simulations are shown in Sec. IV A and Sec. IV B for the bulk material and the device, respectively. We analyze the outcomes

of the simulations and compare them with the experimental measurements, where available. We discuss the influence of compositional non-uniformity on the properties of both the bulk alloy and the device and demonstrate the suitability of our multiscale scheme in giving a proper description of the device behavior accounting for the nanoscale features of the underlying atomistic structure. Note that there are many experimentally observed features of InGaN QWs which have effects of decreasing the band gap and broadening the emission spectrum. Examples which have been considered in previous modelling are variations in the well width and a diffuse upper interface. With our work, we do not intend to rule out these features, which also lead to effects similar to those of clustering. Our intention is to show that non-uniformity in the alloy, even if not so large, could explain some experimental observations. We deliberately did not try to include in our work also well width variations or diffused interfaces, in order to not mix up different effects. Moreover, in the case of maximal clustering, excitonic effects become very important and change the physics of the system[81]. However, we expect not too drastic effects, as long as the system does not evolve into QDs. Also for this reason, we restricted our current study to small deviations from the random alloy case.

A. Characterization of bulk InGaN alloys: compositional non-uniformities induce spatial localization of carriers.

In this section, we show how ETB can properly describe the effects of compositional non-uniformities on the electronic properties of bulk nitride materials. Specifically, we give an example of the ETB approach application to the study of non-uniform InGaN alloys.

InGaN is the most successful material for the realization of green-blue-violet LEDs[14,82] and blue-violet laser diodes[83]. Simulation studies performed assuming a uniform indium distribution within the InGaN alloy[19,20,32,39,78] miss important effects, such as translational symmetry breaking and pronounced carrier localization, induced by compositional non-uniformity. In particular, Chichibu *et al.* have studied the influence of localizing valence states associated with In-N zigzag atomic chains on the emission properties of indium containing nitride alloys, using experimental techniques[84]. Moreover, a theoretical description of the spatial localization of carriers induced by the intrinsic formation of In-N zigzag chains and quantum dots (QD) in InGaN alloys is reported in previous studies[85,86]. However, the mentioned arrangements do not resemble the atomic configuration obtained when only slight to medium deviations from the uniform random alloy structure are taken into account.

In the last year, a novel approach to generate non-uniform random alloy samples has been proposed[24,25] that goes beyond the zigzag and QD-like representation of the non-uniformities. The uniform samples are generated by randomly substituting gallium atoms with indium atoms and assuming a spatially uniform substitution probability equal to the mean indium concentration. For the non-uniform alloy, a certain percentage of indium atoms, denoted as the percentage of uniformity in order to identify the different structures, is uniformly distributed. The remaining indium atoms are then distributed with a spatially varying probability as follows: a gallium atom is picked randomly, then the indium atoms around this gallium are counted up to the second nearest cation site, and the substitution probability is calculated as the ratio of this number and the available cation sites. This is repeated until all necessary indium atoms are distributed and leads to a spatial correlation. Note that the total number of indium atoms is kept constant in order to fix the mean indium content. The degree of clustering can be controlled by the percentage of uniformly distributed indium atoms: the lower the percentage, the more clustering can be expected. The procedure used to generate non-uniform random alloy samples is illustrated in Figure 1 of Supporting Information (SI), for clarity.

Using the mentioned approach, we consider here a $10\times10\times10$ nm^3 $In_xGa_{1-x}N$ supercell at several degrees of non-uniformity. We set the mean indium content to $x = 0.2$, corresponding to a value laying in between those needed to obtain blue and green quantum well light emitting diodes, and we consider the following percentage of uniformity: 100% (random alloy), 80%, 60% and 40%. To obtain the electronic properties, we use the atomistic ETB approach, as implemented in the TiberCAD software[87]. The atomistic structures are first relaxed using the VFF method. Then, we compute the first twelve electron and twenty-four hole states at the Γ point of the Brillouin zone, from which one can calculate also the momentum matrix elements, optical spectra and density of states. To obtain statistically significant results, we simulate 50 structures for the uniform random alloy configuration, as well as for the slightly clustered alloy (80% uniformity). For the other cases, we use 100 random samples since the statistical variations are more pronounced for the strongly clustered structures.

Here, we show how to quantify the spatial localization of carriers associated to the ground state electron and hole wave functions, using an approach similar to the analysis of Chan *et al.*[23]. For a single realization from the ensemble, we first evaluate the projected density of states (PDOS) for each lattice site. This is expressed as $PDOS_k(E) = \sum_m |<\phi_k|\psi_m>|^2\delta(E-E_m)$ where E_m and ψ_m are the eigenvalue and the wave function of the m^{th} state, respectively, and ϕ_k is the atomic orbital of the atom placed at the k^{th} lattice site. Then, we count the number of atoms (NA) with the highest PDOS values that holds 80% of the total density of the considered state, i.e. the electron and hole ground state. The percentage volume is defined as the ratio of NA over the total number of atoms in the supercell. We show the real-space spatial distribution of the ground state electron and hole wave function in Table 5. In particular, the NA atoms that contribute to the 80% of the density of the electron (left column) and hole (right column) ground state are depicted within the supercell for each amount of uniformity. The percentage volume is also indicated. We can see that the hole wave function is far more localized than that of the electron, for all the considered amounts of uniformity, as expected. Furthermore, the localization of both carriers increases for increasing non-uniformity. These results based on empirical tight binding

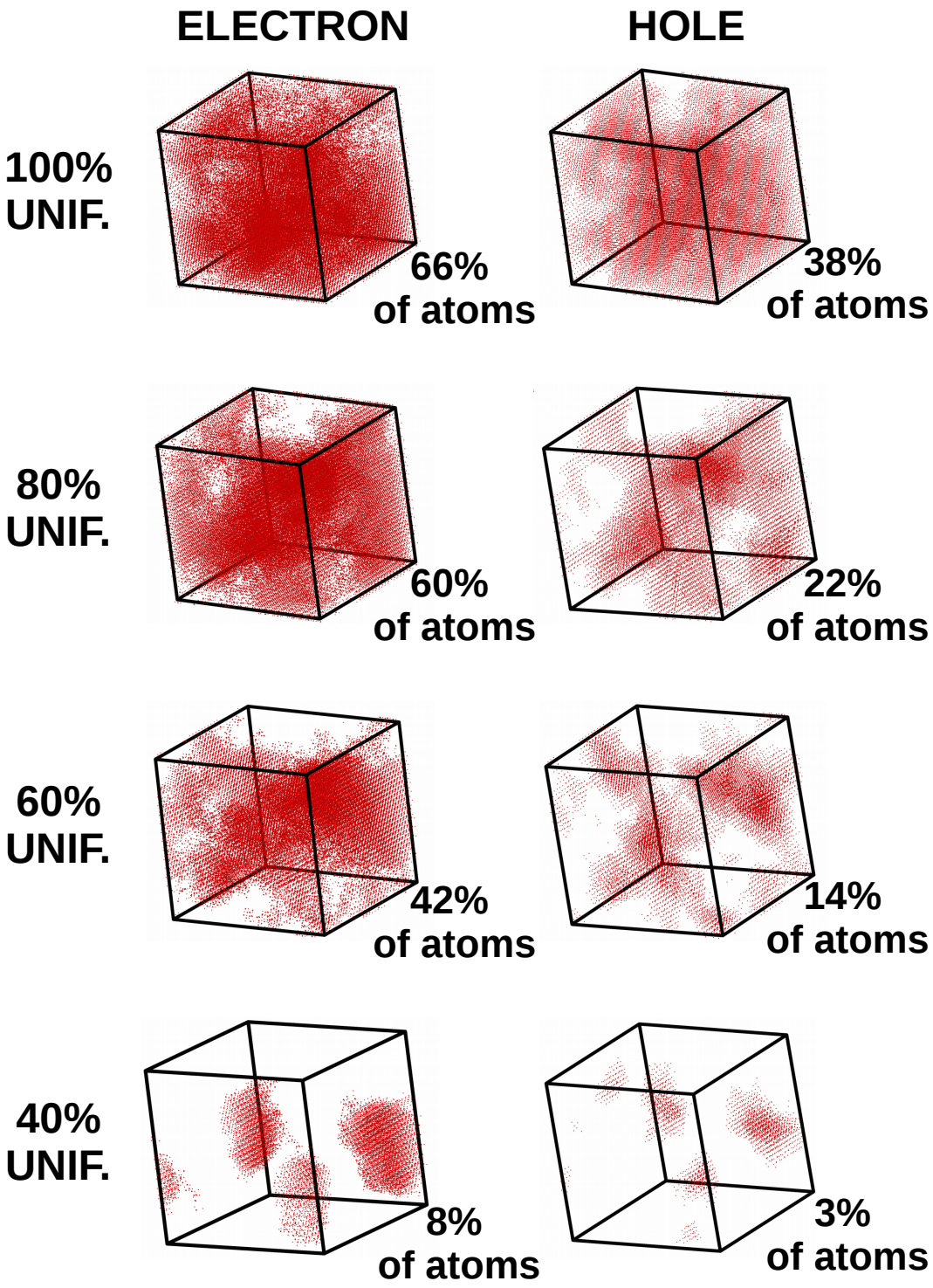

FIG. 5. Real-space spatial distribution of the ground state electron and hole wave function for the considered percentage of uniformity. Only the NA atoms that holds 80% of the density of the considered state are depicted within the supercell. The percentage volume (i.e., the ratio of NA over the total number of atoms in the supercell) is also indicated.

are in good qualitative agreement with the study of Chan *et al.*[23], where empirical pseudopotential method has been used. Note, however, that for higher degree of localization the electrostatic potential is expected to vary more and more spatially, so that strictly speaking a 3D self-consistent simulation should be done. Also, it might become necessary to include excitonic effects, as done e.g. by Roble *et al.*[88] The influence of compositional non-uniformity on the ensemble average of the DOS is discussed in Section II (Figure 2) of SI.

Beside the carrier densities, the DOS and optical properties, a further quantity of interest is the band structure. Especially in random alloy or superlattice calculations, the band structure can visually reveal interesting features of the electronic structure and allows to relate it to the bulk band structure of the constituent materials. While it is conceptually easy to calculate the band structure for periodic supercell calculations, the interpretation is not immediate due to band folding. It is therefore necessary to unfold the calculated supercell band structure into a primitive Brillouin zone, in order to allow an intuitive interpretation and comparison with bulk band structures[89,90]. Several approaches to achieve this have been described in literature. In our implementation, we followed Medeiros *et al.*[91]. Figure 6 shows an example for bulk $In_{0.25}Ga_{0.75}N$, where the calculations have been performed on an $8\times8\times4$ supercell, and the band dispersion has been calculated along $K\rightarrow\Gamma\rightarrow A$. In this example, to obtain a dispersion in the primitive cell Brillouin zone with 49 points, the states in 19 k points of the supercell Brillouin zone have to be computed. It can be seen that the folded band structure, plotted as black lines in the right panel, can be hardly interpreted, while the unfolded one reveals the typical band dispersion of III-nitrides around the Γ-point. In this example, the unfolded band structure reveals that the random alloy fluctuations do not give rise to localized defect states. Rather, their effect on the band structure can be interpreted as random perturbations of an effective virtual crystal, which can substantially be described by an effective band structure. As such, this validates the use of an effective medium approximation like k·p for such a random alloy, and the unfolded band strcture could be used to derive the corresponding k·p parameters.

It has to be noted, however, that it is hard to reconstruct the full band structure for large supercells, since the spectrum gets denser with increasing supercell size and thus more and more states have to be calculated to obtain the energy levels far from the minima. For the unfolded bands in Fig. 6 we used 264 states, although the supercell is relatively small.

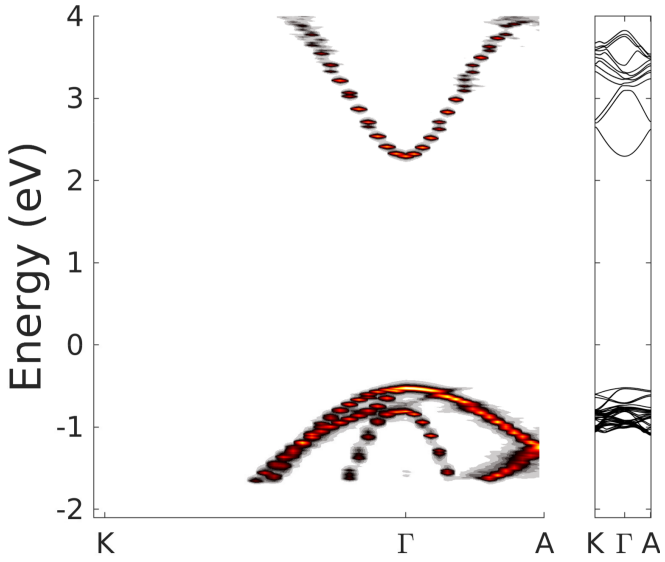

FIG. 6. Unfolded dispersion of an $8\times8\times4$ bulk $In_{0.25}Ga_{0.75}N$ supercell, strained on (0001) GaN. The color scale shows the projection weight of the supercell states onto a state with primitive cell periodicity and given crystal momentum in the primitive cell Brillouin zone. Lighter colors have larger weight, black corresponds to zero. In the right panel the band structure of the same random alloy sample, without unfolding, is shown.

B. Impact of compositional non-uniformity in (In,Ga)N-based light emitting diodes

In order to theoretically study the effect of alloy non-uniformity on macroscopic device performance, we use a computational scheme combining continuum and atomistic models, as described in section III.

We use the InGaN/GaN SQW LED structure shown schematically in Fig. 7a, assuming a mean indium content of $x = 20\%$ and a well width of 3 nm. The considered device has the same structural parameters as those used for the calculations performed by Auf der Maur *et al.*[19], where only a uniform InGaN alloy was addressed. Although spatial variations of the QW thickness can be expected in real LEDs, which influence device behavior as shown e.g. in[27,78], we assumed for this example ideal QW interfaces. Well width variations on short length scale could be taken into account using an approach similar to that in the analysis of Tanner *et al.*[27], but then strain and potentials should also be solved in 3D, due to the explicit structural inhomogeneity in the QW plane.

All simulations have been performed for a LED operating point close to the maximum internal quantum efficiency (IQE). For the atomistic structure, we have chosen a periodic supercell of 10×10 nm^2 in the quantum well plane, including roughly 3 nm of the GaN barrier on each side, leading to a structure with nearly 100000 atoms. To obtain the electrostatic potential, needed to set up the TB Hamiltonian, and the quasi Fermi levels at the chosen operating point, we first solve the 1D Schrödinger/drift-diffusion problem, using TiberCAD software[87]. The potential is then projected onto the atomic positions, neglecting thus variations in the QW plane. The atomistic structures are first relaxed using a Keating VFF method[73]. Then, we compute the first eight electron and twelve hole states in the Γ, M, X and Y points of the reduced Brillouin zone using ETB, and we use the trapezoidal method for reciprocal space integration. The optical spectra and densities are finally obtained by populating the quantum states with the calculated quasi Fermi levels.

The conduction and valence band edge profiles near the maximum IQE operating point, as obtained by 1D Schrödinger/drift-diffusion resolution scheme, are depicted in

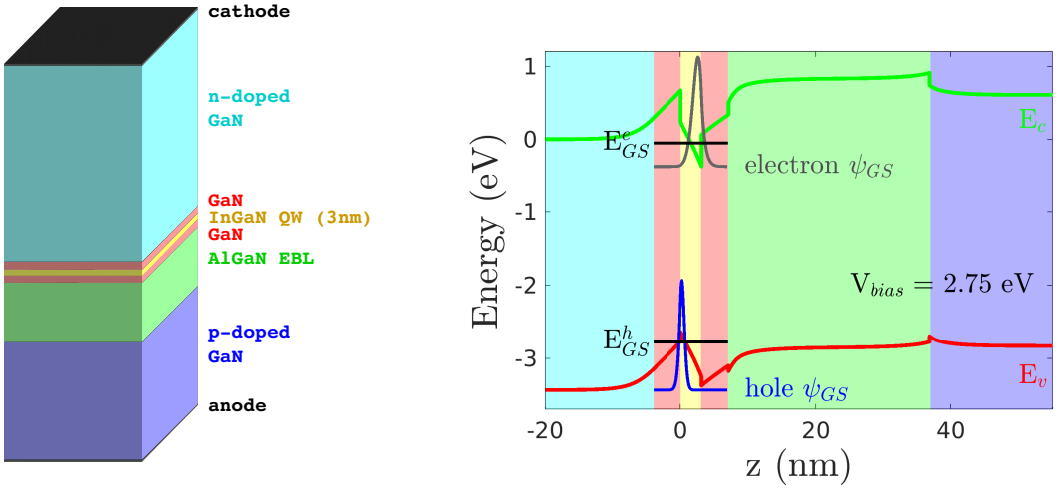

(a) (b)

FIG. 7. a) Schematic view of the simulated structure. b) Conduction and valence band edge profile near the maximum IQE operating point. The ground state wave function and eigenvalue for electron and hole are also reported. The applied bias voltage is 2.75 eV.

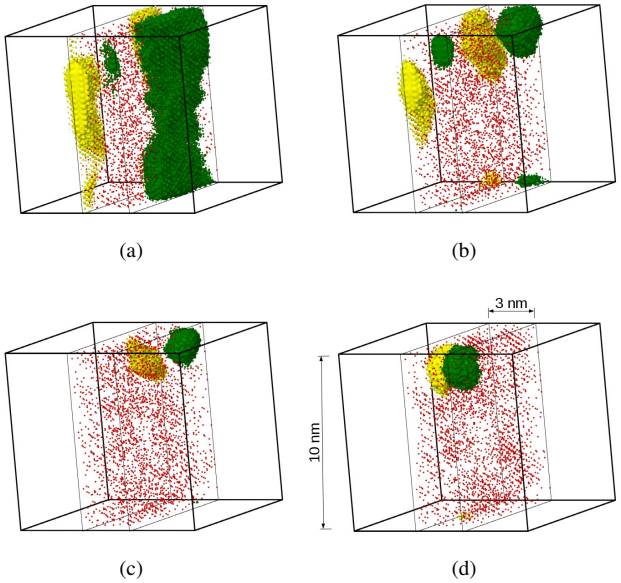

(a) (b) (c) (d)

FIG. 8. The ground state electron (green) and hole (yellow) wave functions for the $In_{0.2}Ga_{0.8}N$ quantum well with 100%, 80%, 60% and 40% of uniformly distributed indium atoms are represented in panel a), b), c) and d), respectively. The isosurfaces containing 50% of the total ground state density are shown. Only indium atoms are depicted in red.

Figure 7b by the green and red lines, respectively. The resulting k·p ground state wave functions for electron (gray) and hole (blue) are also reported, showing how the carriers are localized at opposite sides of the InGaN QW. Different regions of the device are identified by different colors, with reference to Figure 7a.

The ground state electron (green) and hole (yellow) wave functions derived by ETB calculations for one sample structure with increasing degree of clustering are illustrated in Figure 8a-d. As already observed in Figure 5, the localization of both carriers increases for increasing non-uniformity. Moreover, with substantial alloy non-uniformity, the indium clustering may localize both electrons and holes in the same spatial position, overcoming the QCSE, as is the case in the last panel of Figure 8. Otherwise, due to QCSE, the electron and hole states are influenced by the largely independent indium content fluctuations near the lower and upper QW interface, respectively[19]. As mentioned earlier, however, for large non-uniformity the in-plane potential variations should be included in the model, so that the potentials have to be solved in 3 dimensions, too.

In Figure 9a, the emission spectra of the InGaN/GaN QW are shown for all the considered percentage of uniformity in the indium atoms distribution. Note that the represented spectra result from the average over the 50 to 100 simulated random samples (see Section IV A). The effect of the non-uniformity in the alloy composition is to induce a red-shift of the peak emission energy, in agreement with the band gap reduction detected by experimental and theoretical techniques[24,25] when the presence of indium clusters is taken into account. Moreover, it can be seen in Figure 9a that indium clustering yields a pronounced broadening of the emission spectrum. We compared our results with the available measurements reported in literature[92] for a SQW LED structure similar to the simulated one but with a slightly lower indium content, represented by the red area in Figure 9a. Notably, both the measured peak position and spectrum width are well described when the 60% of uniformity in the indium atoms distribution is considered. In particular, the high energy tail is well reproduced, while the low energy tail shows slightly too little broadening. Note that the 60% uniform samples are consistent with the atom probe tomography (APT) measurements reported in literature[21,78] if the limited APT detection

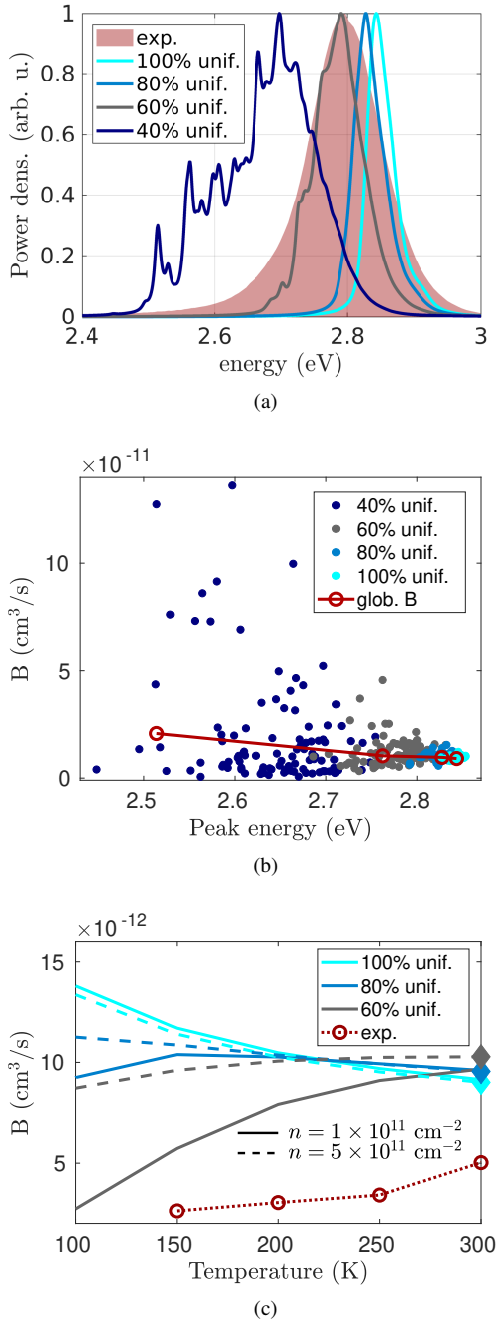

FIG. 9. a) Calculated emission spectra (sample average) for an $In_{0.2}Ga_{0.8}N$ quantum well at several percentage of uniformity. The experimental spectrum[92] is depicted by the red area. b) Radiative recombination coefficient B of an $In_{0.2}Ga_{0.8}N$ quantum well for several percentage of uniformity. The results, derived for a mean carrier density of 5×10^{11} cm^{-2} and a temperature of 300 K, for each simulated sample are visualized as dots and the global B is labeled by red circles. c) Temperature dependence of B for an $In_{0.2}Ga_{0.8}N$ quantum well at several percentage of uniformly distributed indium atoms. The solid and dashed lines represent the values obtained for a mean carrier density of 10^{11} and 5×10^{11} cm^{-2}, respectively. The experimental behavior[37] derived for a mean carrier density of approximately 10^{12} cm^{-2} is labeled by red circles. The results for the 40% uniform structure are not reported in the figure, since their range of variation is too wide. The global B values of Figure 8b are depicted by diamond-shaped markers.

efficiency is taken into account[93]. This is discussed elsewhere in more detail[25].

One of the figures of merit usually used to determine the performance of LED devices is the internal quantum efficiency (IQE), which is the ratio between radiative and total recombination. Radiative recombination is usually modelled as $R_r = Bnp$, where B is the radiative recombination parameter and n and p the electron and hole densities[94]. The parameter B can be measured for example by time resolved photoluminescence or differential life time analysis[95,96], but it can also be extracted from the simulation, allowing thus for a direct comparison. From the simulations on a statistical ensemble of random structures we can obtain a value for B for each single random structure, and global one. The latter is the one we compare with the experimental data. In order to derive the value of B of each random sample, we assumed constant quasi Fermi levels, chosen such that the mean carrier density is also kept constant and equal to $\bar{n} = \bar{p} = 5 \times 10^{11}$ cm^{-2}, where the mean value is calculated over the ensemble of structures. Then we defined the global radiative coefficient as $\bar{B} = \bar{R}_r/(\bar{n}\bar{p})$, where $\bar{R}_r$ is the weighted sum of the radiative recombination rate of all random samples[19]. The obtained values of B for all the simulated structures and each considered percentage of uniformity are shown in Figure 9b. It can be seen that the presence of indium clusters induces an increment of the spread in the calculated B values and of the derived global radiative coefficient. In fact, for increasing non-uniformity, a higher number of optical transitions is allowed due to the translational symmetry breaking caused by the presence of disorder[25]. Such an effect yields an increment of the radiative coefficient value when the non-uniformity of the structure increases. Furthermore, the increase of the global B suggests the onset of the transition from QW to QD-like behavior, as confirmed by the localization of the wave functions discussed in Figure 8.

Finally, it is interesting to study how the compositional non-uniformity qualitatively affects the temperature dependence of the radiative coefficient. In fact, simple QW theory predicts B to be proportional to the inverse of the temperature[97]. However, this is in contrast with the experimental behavior[37] that shows increasing values of B when the temperature is incremented. The temperature dependence of the global B is shown in Figure 9c for several values of the mean carrier density. Note that, in order to derive the occupation of the states at each considered temperature, we adjusted the quasi Fermi levels so that the mean carrier density is kept constant. Moreover, instead of performing calculations at each temperature, we merely reoccupy the states calculated once. This certainly introduces some inaccuracy, however it is enough to predict the qualitative trends.

We can see that only the trend obtained for the 100% uniform structure agrees with standard QW theory, i.e. the radiative coefficient $\bar{B}$ decreases with increasing temperature for all the considered values of the mean carrier density. On the other hand, when the non-uniformity of the alloy composition is addressed, the temperature behavior of $\bar{B}$ becomes mostly constant or even increasing with temperature, in net contrast with theory. Interestingly, the trend derived for the 60% uniform

structure with $\bar{n} = 5 \times 10^{11}$ cm^{-2} better matches the measured data by Nippert et al.[37] for a blue multi quantum well LED, reported in Figure 9c by red circles, which presumably had slightly different indium content and active layer structure.

The effect of clustering and temperature on the behaviour of the radiative coefficient is further discussed in Section III (Figures S3 and S4) of SI.

V. CONCLUSIONS

We have presented an overview on different approaches to model the influence of statistical alloy fluctuations on the performance of electronic devices, with special focus on III-nitride LEDs, where this topic is currently of particular interest. While empirical analytic models and continuum quantum mechanical approaches can provide good qualitative and even quantitative results, they suffer from the fact that the atomic configuration does not enter directly the model. Or it has to be parameterized, by defining a localization energy for example, or it enters via a compositional alloy profile. In order to directly correlate the atomic structure to the optoelectronic device properties, atomistic models can be more suitable. Among the different possibilities, ETB has proven to be a good compromise, so that several research groups are using different versions of ETB for the study of carrier localization in nitride LEDs in the visible and UV. As an important point, we described the necessity to embed the atomistic scale model in a continuum device model by means of multiple scale linking or coupling, since on the one hand the atomic model cannot be applied to the whole device, and on the other hand the simulation results have to be obtained for realistic operating conditions in order to be compared with measurements.

The usefulness of the combined TB/device modeling approach has been illustrated with simulation examples for bulk InGaN and InGaN/GaN QW LEDs, but it is also proven by the available literature from different groups.

One of the main drawbacks of calculating the electronic and optical properties from eigenstates of an ETB Hamiltonian lies in the fact that, for the required supercell size, a high number of states have to be computed. This is particularly relevant if a self-consistent solution is sought. It is therefore important to further optimize the efficiency of the eigensolvers, or to resort to alternative schemes. In this regard, it might be possible to apply the newly developed potential landscape theory to the ETB Hamiltonian. Nevertheless, we can conclude that at the current stage the combination of the relatively efficient ETB and device modeling constitutes a reliable modeling tool, providing valuable insight into device physics related to alloy disorder in III-nitrides.

SUPPLEMENTARY MATERIAL

The Supplementary Material provides additional information and illustrative figures on the generation of non-uniform alloys, on the band tails as a function of alloy uniformity, on the influence of non-uniformity on the predicted radiative recombination parameter, and on the variation of the ETB ground state energies, when the potential profile induced by piezoelectric polarization is calculated in 3D based on continuum elasticity with locally extracted mean indium concentration.

ACKNOWLEDGMENTS

We wish to acknowledge the support of Horizon 2020 project ChipScope, under grant agreement number 737089.

DATA AVAILABILITY STATEMENT

The data that support the findings of this study are available from the corresponding author upon reasonable request.

[1] C. De Falco, E. Gatti, A. L. Lacaita, and R. Sacco, "Quantum-corrected drift-diffusion models for transport in semiconductor devices," Journal of Computational Physics **204**, 533–561 (2005).
[2] S. Yamakawa, S. Goodnick, S. Aboud, and M. Saraniti, "Quantum corrected full-band cellular Monte Carlo simulation of AlGaN/GaN HEMTs," Journal of Computational Electronics **3**, 299–303 (2004).
[3] L. Shifren, C. Ringhofer, and D. Ferry, "A Wigner function-based quantum ensemble Monte Carlo study of a resonant tunneling diode," IEEE Transactions on Electron Devices **50**, 769–773 (2003).
[4] A. Pecchia and A. Di Carlo, "Atomistic theory of transport in organic and inorganic nanostructures," Reports on Progress in Physics **67**, 1497 (2004).
[5] A. Di Carlo, "Microscopic theory of nanostructured semiconductor devices: beyond the envelope-function approximation," Semiconductor Science and Technology **18**, R1 (2002).
[6] V. Fiorentini, F. Bernardini, F. Della Sala, A. Di Carlo, and P. Lugli, "Effects of macroscopic polarization in III-V nitride multiple quantum wells," Physical Review B **60**, 8849 (1999).
[7] M. Auf der Maur, "Multiscale approaches for the simulation of InGaN/GaN LEDs," Journal of Computational Electronics **14**, 398–408 (2015).
[8] M. Auf der Maur, A. Pecchia, G. Penazzi, F. Sacconi, and A. Di Carlo, "Coupling atomistic and continuous media models for electronic device simulation," Journal of Computational Electronics **12**, 553–562 (2013).
[9] C. Yam, L. Meng, G. Chen, Q. Chen, and N. Wong, "Multiscale quantum mechanics/electromagnetics simulation for electronic devices," Physical Chemistry Chemical Physics **13**, 14365–14369 (2011).
[10] S. Steiger, M. Povolotskyi, H.-H. Park, T. Kubis, and G. Klimeck, "NEMO5: A parallel multiscale nanoelectronics modeling tool," IEEE Transactions on Nanotechnology **10**, 1464–1474 (2011).
[11] J. Guo, S. Datta, M. Lundstrom, and M. Anantam, "Toward multiscale modeling of carbon nanotube transistors," International Journal for Multiscale Computational Engineering **2** (2004).
[12] G. Klimeck, "Quantum and semi-classical transport in NEMO 1-D," Journal of Computational Electronics **2**, 177–182 (2003).
[13] Y. Xu and N. R. Aluru, "Multiscale electrostatic analysis of silicon nanoelectromechanical systems (NEMS) via heterogeneous quantum models," Physical Review B **77**, 075313 (2008).
[14] S. Nakamura, M. Senoh, and T. Mukai, "P-GaN/n-InGaN/n-GaN double-heterostructure blue-light-emitting diodes," Japanese Journal of Applied Physics **32**, L8–L11 (1993).
[15] S. Nakamura, "Present performance of InGaN-based blue/green/yellow LEDs," in *Light-Emitting Diodes: Research, Manufacturing, and Applications*, Vol. 3002 (International Society for Optics and Photonics, 1997) pp. 26–36.
[16] H.-M. Kim, Y.-H. Cho, H. Lee, S. I. Kim, S. R. Ryu, D. Y. Kim, T. W. Kang, and K. S. Chung, "High-Brightness Light Emitting Diodes Using Dislocation-Free Indium Gallium Nitride/Gallium Nitride Multiquantum-Well Nanorod Arrays," Nano Letters **4**, 1059–1062 (2004).

[17] E. Taylor, P. R. Edwards, and R. W. Martin, "Colorimetry and efficiency of white LEDs: Spectral width dependence," physica status solidi (a) **209**, 461–464 (2012).

[18] J. Piprek, "Efficiency droop in nitride-based light-emitting diodes," physica status solidi (a) **207**, 2217–2225 (2010).

[19] M. Auf der Maur, A. Pecchia, G. Penazzi, W. Rodrigues, and A. Di Carlo, "Efficiency drop in green InGaN/GaN light emitting diodes: The role of random alloy fluctuations," Phys. Rev. Lett. **116**, 027401 (2016).

[20] C. M. Jones, C.-H. Teng, Q. Yan, P.-C. Ku, and E. Kioupakis, "Impact of carrier localization on recombination in InGaN quantum wells and the efficiency of nitride light-emitting diodes: Insights from theory and numerical simulations," Applied Physics Letters **111**, 113501 (2017).

[21] M. J. Galtrey, R. A. Oliver, M. J. Kappers, C. J. Humphreys, D. J. Stokes, P. H. Clifton, and A. Cerezo, "Three-dimensional atom probe studies of an $In_xGa_{1-x}N$/GaN multiple quantum well structure: Assessment of possible indium clustering," Applied Physics Letters **90**, 061903 (2007).

[22] M. J. Galtrey, R. A. Oliver, M. J. Kappers, C. J. Humphreys, P. H. Clifton, A. Cerezo, and G. D. W. Smith, "Response to "Comment on 'Three-dimensional atom probe studies of an $In_xGa_{1-x}N$/GaN multiple quantum well structure: assessment of possible indium clustering'"," Applied Physics Letters **91**, 176102 (2007).

[23] J. A. Chan, J. Z. Liu, and A. Zunger, "Bridging the gap between atomic microstructure and electronic properties of alloys: The case of (In,Ga)N," Phys. Rev. B **82**, 045112 (2010).

[24] A. Di Vito, A. Pecchia, A. Di Carlo, and M. Auf der Maur, "Characterization of non-uniform InGaN alloys: spatial localization of carriers and optical properties," Japanese Journal of Applied Physics **58**, SCCC03 (2019).

[25] A. Di Vito, A. Pecchia, A. Di Carlo, and M. Auf der Maur, "Impact of Compositional Nonuniformity in (In, Ga) N-Based Light-Emitting Diodes," Physical Review Applied **12**, 014055 (2019).

[26] S. Karpov, "Carrier localization in InGaN by composition fluctuations: Implication to the "green gap"," Photonics Research **5**, A7–A12 (2017).

[27] D. S. P. Tanner, J. M. McMahon, and S. Schulz, "Interface Roughness, Carrier Localization, and Wave Function Overlap in *c*-Plane $(In,Ga)N/GaN$ Quantum Wells: Interplay of Well Width, Alloy Microstructure, Structural Inhomogeneities, and Coulomb Effects," Phys. Rev. Applied **10**, 034027 (2018).

[28] M. Piccardo, C.-K. Li, Y.-R. Wu, J. Speck, B. Bonef, R. Farrell, M. Filoche, L. Martinelli, J. Peretti, and C. Weisbuch, "Localization landscape theory of disorder in semiconductors. II. Urbach tails of disordered quantum well layers," Physical Review B **95** (2017), 10.1103/PhysRevB.95.144205.

[29] S. Schulz, M. A. Caro, C. Coughlan, and E. P. O'Reilly, "Atomistic analysis of the impact of alloy and well-width fluctuations on the electronic and optical properties of InGaN/GaN quantum wells," Phys. Rev. B **91**, 035439 (2015).

[30] A. David, N. G. Young, and M. D. Craven, "Many-Body Effects in Strongly Disordered III-Nitride Quantum Wells: Interplay Between Carrier Localization and Coulomb Interaction," Phys. Rev. Applied **12**, 044059 (2019).

[31] K. H. Baloch, A. C. Johnston-Peck, K. Kisslinger, E. A. Stach, and S. Gradečak, "Revisiting the "In-clustering" question in InGaN through the use of aberration-corrected electron microscopy below the knock-on threshold," Applied Physics Letters **102**, 191910 (2013).

[32] T.-J. Yang, R. Shivaraman, J. S. Speck, and Y.-R. Wu, "The influence of random indium alloy fluctuations in indium gallium nitride quantum wells on the device behavior," Journal of Applied Physics **116**, 113104 (2014).

[33] M. López, A. Pecchia, M. Auf der Maur, F. Sacconi, G. Penazzi, and A. Di Carlo, "Atomistic simulations of InGaN/GaN random alloy quantum well LEDs," physica status solidi c **11**, 632–634 (2014).

[34] P. R. C. Kent and A. Zunger, "Carrier localization and the origin of luminescence in cubic InGaN alloys," Applied Physics Letters **79**, 1977–1979 (2001).

[35] M. A. Caro, S. Schulz, and E. P. O'Reilly, "Theory of local electric polarization and its relation to internal strain: Impact on polarization potential and electronic properties of group-III nitrides," Phys. Rev. B **88**, 214103 (2013).

[36] Z. Li, J. Kang, B. Wei Wang, H. Li, Y. Hsiang Weng, Y.-C. Lee, Z. Liu, X. Yi, Z. Chuan Feng, and G. Wang, "Two distinct carrier localization in green light-emitting diodes with InGaN/GaN multiple quantum wells," Journal of Applied Physics **115**, 083112 (2014).

[37] F. Nippert, S. Y. Karpov, G. Callsen, B. Galler, T. Kure, C. Nenstiel, M. R. Wagner, M. Straßburg, H.-J. Lugauer, and A. Hoffmann, "Temperature-dependent recombination coefficients in InGaN light-emitting diodes: Hole localization, Auger processes, and the green gap," Applied Physics Letters **109**, 161103 (2016).

[38] B. Lee and L. W. Wang, "Band gap bowing and electron localization of $Ga_xIn_{1-x}N$," Journal of Applied Physics **100**, 093717 (2006).

[39] D. Oriato and A. B. Walker, "Effects of piezoelectric field, bias and indium fluctuations on a InGaN–GaN single quantum well system," Physica B: Condensed Matter **314**, 59 – 62 (2002), proceedings of the Twelfth International Conference on Nonequilib rium Carrier Dynamics in Semiconductors.

[40] X. Wu, E. J. Walter, A. M. Rappe, R. Car, and A. Selloni, "Hybrid density functional calculations of the band gap of $Ga_xIn_{1-x}N$," Phys. Rev. B **80**, 115201 (2009).

[41] I. Gorczyca, S. P. Łepkowski, T. Suski, N. E. Christensen, and A. Svane, "Influence of indium clustering on the band structure of semiconducting ternary and quaternary nitride alloys," Phys. Rev. B **80**, 075202 (2009).

[42] S. L. Chuang and C. Chang, "$\mathbf{k}\cdot\mathbf{p}$ method for strained wurtzite semiconductors," Physical Review B **54**, 2491 (1996).

[43] S. L. Chuang, *Physics of optoelectronic devices*, 1st ed. (Wiley Series in Pure and Applied Optics, 1995).

[44] L. C. L. Y. Voon and M. Willatzen, *The kp method: electronic properties of semiconductors* (Springer Science & Business Media, 2009).

[45] S. Karpov, "Effect of carrier localization on recombination processes and efficiency of InGaN-based LEDs operating in the "green gap"," Applied Sciences (Switzerland) **8** (2018), 10.3390/app8050818.

[46] M. Filoche, M. Piccardo, Y.-R. Wu, C.-K. Li, C. Weisbuch, and S. Mayboroda, "Localization landscape theory of disorder in semiconductors. I. Theory and modeling," Physical Review B **95** (2017), 10.1103/PhysRevB.95.144204.

[47] D. Chaudhuri, J. C. Kelleher, M. R. O'Brien, E. P. O'Reilly, and S. Schulz, "Electronic structure of semiconductor nanostructures: A modified localization landscape theory," Physical Review B **101** (2020), 10.1103/physrevb.101.035430.

[48] T.-Y. Tsai, K. Michalczewski, P. Martyniuk, C.-H. Wu, and Y.-R. Wu, "Application of localization landscape theory and the $k\cdot p$ model for direct modeling of carrier transport in a type II superlattice InAs/InAsSb photoconductor system," Journal of Applied Physics **127** (2020), 10.1063/1.5131470.

[49] H.-H. Chen, J. Speck, C. Weisbuch, and Y.-R. Wu, "Three dimensional simulation on the transport and quantum efficiency of UVC-LEDs with random alloy fluctuations," Applied Physics Letters **113** (2018), 10.1063/1.5051081.

[50] A. V. Krukau, O. A. Vydrov, A. F. Izmaylov, and G. E. Scuseria, "Influence of the exchange screening parameter on the performance of screened hybrid functionals," The Journal of chemical physics **125**, 224106 (2006).

[51] M. S. Hybertsen and S. G. Louie, "Electron correlation in semiconductors and insulators: Band gaps and quasiparticle energies," Physical Review B **34**, 5390 (1986).

[52] S. Ismail-Beigi and S. G. Louie, "Excited-state forces within a first-principles Green's function formalism," Physical review letters **90**, 076401 (2003).

[53] M. C. Payne, M. P. Teter, D. C. Allan, T. Arias, and a. J. Joannopoulos, "Iterative minimization techniques for ab initio total-energy calculations: molecular dynamics and conjugate gradients," Reviews of modern physics **64**, 1045 (1992).

[54] C. M. C M Goringey, D. R. Bowlerykand, and M. Hernandez, "Tight-binding modelling of materials," Rep. Prog. Phys. **60**, 1447–1512 (1997).

[55] A. Di Carlo, "Microscopic theory of nanostructured semiconductor devices: beyond the envelope-function approximation," Semiconductor Science and Technology **18**, R1–R31 (2003).

[56] T. Boykin, "Recent developments in tight-binding approaches for nanowires," J. Comput. Electron. **8(2)**, 142 (2009).

[57] F. Oyafuso, G. Klimeck, R. C. Bowen, and T. B. Boykin, "Atomistic electronic structure calculations of unstrained alloyed systems consisting of a million atoms," Journal of Computational electronics **1**, 317–321 (2002).

[58] D. J. Chadi, "Spin-orbit splitting in crystalline and compositionally disordered semiconductors," Phys. Rev. B **16**, 790 (1977).

[59] J.-M. Jancu, R. Scholz, F. Beltram, and F. Bassani, "Empirical spds* tight-binding calculation for cubic semiconductors: General method and material parameters," Phys. Rev. B **57**, 6493–6507 (1998).

[60] F. Raouafi, B. Chamekh, J. Even, and J.-M. Jancu, "Electronic and Optical Properties in the Tight-Binding Method," (2014).

[61] T. B. Boykin, G. Klimeck, R. C. Bowen, and F. Oyafuso, "Diagonal parameter shifts due to nearest-neighbor displacements in empirical tight-binding theory," Physical Review B **66** (2002), 10.1103/physrevb.66.125207.

[62] J.-M. Jancu, F. Bassani, F. D. Sala, and R. Scholz, "Transferable tight-binding parametrization for the group-III nitrides," Applied Physics Letters **81**, 4838–4840 (2002).

[63] Y.-M. Niquet and C. Delerue, "Band offsets, wells, and barriers at nanoscale semiconductor heterojunctions," Physical Review B **84**, 075478 (2011).

[64] S.-H. Wei and A. Zunger, "Valence band splittings and band offsets of AlN, GaN, and InN," Applied Physics Letters **69**, 2719–2721 (1996).

[65] C.-F. Shih, N.-C. Chen, P.-H. Chang, and K.-S. Liu, "Band offsets of InN/GaN interface," Japanese Journal of Applied Physics **44**, 7892–7895 (2005).

[66] M. A. Caro, S. Schulz, and E. P. O'Reilly, "Theory of local electric polarization and its relation to internal strain: Impact on polarization potential and electronic properties of group-III nitrides," Physical Review B **88** (2013), 10.1103/physrevb.88.214103.

[67] S. Schulz, M. A. Caro, C. Coughlan, and E. P. O'Reilly, "Atomistic analysis of the impact of alloy and well-width fluctuations on the electronic and optical properties of InGaN/GaN quantum wells," Physical Review B **91** (2015), 10.1103/physrevb.91.035439.

[68] D. S. P. Tanner, M. A. Caro, E. P. O'Reilly, and S. Schulz, "Random alloy fluctuations and structural inhomogeneities in c-plane InxGa1-xN quantum wells: theory of ground and excited electron and hole states," RSC Advances **6**, 64513–64530 (2016).

[69] D. S. P. Tanner, J. M. McMahon, and S. Schulz, "Interface roughness, carrier localization, and wave function overlap in c -plane (In,Ga)N/GaN quantum wells: Interplay of well width, alloy microstructure, structural inhomogeneities, and Coulomb effects," Physical Review Applied **10** (2018), 10.1103/physrevapplied.10.034027.

[70] M. Auf Der Maur, M. Povolotskyi, F. Sacconi, A. Pecchia, G. Romano, G. Penazzi, and A. Di Carlo, "TiberCAD: Towards multiscale simulation of optoelectronic devices," Optical and Quantum Electronics **40**, 1077–1083 (2008).

[71] M. Auf der Maur, G. Penazzi, G. Romano, F. Sacconi, A. Pecchia, and A. Di Carlo, "The multiscale paradigm in electronic device simulation," IEEE Transactions on Electron Devices **58**, 1425–1432 (2011).

[72] T. Koprucki, T. Streckenbach, P. Farrell, O. Marquardt, D. Chaudhuri, M. O'Donovan, S. Patra, and S. Schulz, "Towards multiscale modeling of III-N-based LEDs," in *Numerical Simulation of Optoelectronic Devices (NUSOD) 2019* (2019).

[73] D. Camacho and Y. Niquet, "Application of Keating's valence force field model to non-ideal wurtzite materials," Physica E: Low-dimensional Systems and Nanostructures **42**, 1361 – 1364 (2010).

[74] S. Datta, *Electronic Transport in Mesoscopic Systems* (Cambridge University Press, 1995).

[75] J. Geng, P. Sarangapani, K.-C. Wang, E. Nelson, B. Browne, C. Wordelman, J. Charles, Y. Chu, T. Kubis, and G. Klimeck, "Quantitative Multi-Scale, Multi-Physics Quantum Transport Modeling of GaN-Based Light Emitting Diodes," physica status solidi (a) **215**, 1700662 (2018).

[76] A. Shedbalkar, Z. Andreev, and B. Witzigmann, "Simulation of an indium gallium nitride quantum well light-emitting diode with the non-equilibrium Green's function method," physica status solidi (b) **253**, 158–163 (2016).

[77] C.-K. Li, C.-K. Wu, C.-C. Hsu, L.-S. Lu, H. Li, T.-C. Lu, and Y.-R. Wu, "3D numerical modeling of the carrier transport and radiative efficiency for InGaN/GaN light emitting diodes with V-shaped pits," AIP Advances **6**, 055208 (2016), https://doi.org/10.1063/1.4950771.

[78] D. Watson-Parris, M. J. Godfrey, P. Dawson, R. A. Oliver, M. J. Galtrey, M. J. Kappers, and C. J. Humphreys, "Carrier localization mechanisms in $In_xGa_{1-x}N$/GaN quantum wells," Phys. Rev. B **83**, 115321 (2011).

[79] T. S. S. Chichibu, T. Azuhata and S. Nakamura, Applied Physics Letters **70(21)**, 2822 (1997).

[80] R. Butté, L. Lahourcade, T. K. Uždavinys, G. Callsen, M. Mensi, M. Glauser, G. Rossbach, D. Martin, J.-F. Carlin, S. Marcinkevičius, and N. Grandjean, "Optical absorption edge broadening in thick InGaN layers: Random alloy atomic disorder and growth mode induced fluctuations," Applied Physics Letters **112**, 032106 (2018).

[81] A. Hangleiter, "Recombination of correlated electron-hole pairs in two-dimensional semiconductors," Physical Review B **48**, 9146 (1993).

[82] T. M. S. Nakamura and M. Senoh, Applied Physics Letters **64(13)**, 1687 (1994).

[83] S. Nakamura, M. Senoh, S. I. Nagahama, N. Iwasa, T. Yamada, T. Matsushita, H. Kiyoku, and Y. Sugimoto, Japanese Journal of Applied Physics **35(1B)**, L74 (1996).

[84] S. C. *et al.*, Nature Materials **5**, 810 (2006).

[85] P. Kent and A. Zunger, Applied Physics Letters **79(13)**, 1977 (2001).

[86] L.-W. Wang, Physical Review B **63**, 245107 (2001).

[87] "TiberCAD simulation package," `http://www.tibercad.org`.

[88] A. Roble, S. Patra, F. Massabuau, M. Frentrup, M. Leontiadou, P. Dawson, M. Kappers, R. Oliver, D. Graham, and S. Schulz, "Impact of alloy fluctuations and Coulomb effects on the electronic and optical properties of c-plane GaN/AlGaN quantum wells," Scientific Reports **9** (2019), 10.1038/s41598-019-53693-2.

[89] P. Allen, T. Berlijn, D. Casavant, and J. Soler, "Recovering hidden Bloch character: Unfolding electrons, phonons, and slabs," Physical Review B - Condensed Matter and Materials Physics **87** (2013), 10.1103/PhysRevB.87.085322.

[90] M. Farjam, "Projection operator approach to unfolding supercell band structures," (2015), arXiv:1504.04937 [cond-mat.mtrl-sci].

[91] P. Medeiros, S. Stafström, and J. Björk, "Effects of extrinsic and intrinsic perturbations on the electronic structure of graphene: Retaining an effective primitive cell band structure by band unfolding," Physical Review B - Condensed Matter and Materials Physics **89** (2014), 10.1103/PhysRevB.89.041407.

[92] M. Auf der Maur, B. Galler, I. Pietzonka, M. Strassburg, H. Lugauer, and A. Di Carlo, "Trap-assisted tunneling in InGaN/GaN single-quantum-well light-emitting diodes," Applied Physics Letters **105**, 133504 (2014).

[93] L. Rigutti, L. Mancini, D. Hernández-Maldonado, W. Lefebvre, E. Giraud, R. Butté, J. F. Carlin, N. Grandjean, D. Blavette, and F. Vurpillot, "Statistical correction of atom probe tomography data of semiconductor alloys combined with optical spectroscopy: The case of $Al_{0.25}Ga_{0.75}N$," Journal of Applied Physics **119**, 105704 (2016).

[94] S. Karpov, "ABC-model for interpretation of internal quantum efficiency and its droop in III-nitride LEDs: a review," Optical and Quantum Electronics **47**, 1293–1303 (2015).

[95] F. Nippert, S. Karpov, I. Pietzonka, B. Galler, A. Wilm, T. Kure, C. Nenstiel, G. Callsen, M. Straßburg, H.-J. Lugauer, and A. Hoffmann, "Determination of recombination coefficients in InGaN quantum-well light-emitting diodes by small-signal time-resolved photoluminescence," Japanese Journal of Applied Physics **55**, 05FJ01 (2016).

[96] A. David, N. G. Young, C. Lund, and M. D. Craven, "Review—The Physics of Recombinations in III-Nitride Emitters," ECS Journal of Solid State Science and Technology **9** (2020), 10.1149/2.0372001JSS.

[97] P. K. Basu, *Theory of optical processes in semiconductors: bulk and microstructures*, Vol. 4 (Clarendon press, 1997).